Superalgebraically Convergent Smoothly-Windowed Lattice Sums for Doubly Periodic Green Functions in Three-Dimensional Space

Oscar P. Bruno[*], Stephen P. Shipman[†], Catalin Turc[‡], Stephanos Venakides[§]

Abstract

This paper, Part I in a two-part series, presents *(i)* A simple and highly efficient algorithm for evaluation of quasi-periodic Green functions, as well as *(ii)* An associated boundary-integral equation method for the numerical solution of problems of scattering of waves by doubly periodic arrays of scatterers in three-dimensional space. Except for certain "Wood frequencies" at which the quasi-periodic Green function ceases to exist, the proposed approach, which is based on use of smooth windowing functions, gives rise to lattice sums which converge superalgebraically fast—that is, faster than any power of the number of terms used—in sharp contrast with the extremely slow convergence exhibited by the corresponding sums in absence of smooth windowing. (The Wood-frequency problem is treated in Part II.[1]) A proof presented in this paper establishes rigorously the superalgebraic convergence of the windowed lattice sums. A variety of numerical results demonstrate the practical efficiency of the proposed approach.

Keywords: scattering, periodic Green function, lattice sum, smooth truncation, super-algebraic convergence, boundary-integral equations.

[*]Applied and Computational Mathematics, Caltech, Pasadena, CA 91125. Email: obruno@caltech.edu

[†]Dept. of Mathematics, Louisiana State University, Baton Rouge, LA 70803. Email: shipman@math.lsu.edu

[‡]Dept. of Math. Sciences, New Jersey Inst. of Technology, Newark, NJ 07102. Email: catalin.c.turc@njit.edu

[§]Dept. of Mathematics, Duke University, Durham, NC 27708. Email: ven@math.duke.edu

[1]A preliminary version of Part II can be found in section 4 of arXiv:1307.1176v1.

1 Introduction

The numerical solution of problems of electromagnetic, acoustic and elastic wave scattering by doubly periodic structures entails significant difficulties. Assuming harmonic temporal dependence with frequency ω, the scattered fields can be obtained by means of numerical methods based on integral equations—provided a corresponding numerical scheme is used to evaluate the classical radiating quasi-periodic Green function G^{qper} for the three-dimensional scalar Helmholtz operator $H[u] = \Delta u + k^2 u$ ($k = \omega/c$ where c is the propagation speed). The aforementioned difficulties arise, to a significant extent, from corresponding challenges posed by the evaluation of the quasi-periodic Green function.

The quasi-periodic Green function G^{qper} can be constructed as an infinite sum of free-space Green functions (Helmholtz monopoles) with bi-periodically distributed monopole singularities. Let $\mathbf{v}_1$ and $\mathbf{v}_2$ denote two independent vectors in $\mathbb{R}^2$ that characterize the periodicity, and let $\mathbf{v}_1^*$ and $\mathbf{v}_2^*$ be the dual vectors, that is $\mathbf{v}_i^* \cdot \mathbf{v}_j = \delta_{ij}$. The Bloch wavevector will be denoted by $\mathbf{k} = \alpha \mathbf{v}_1^* + \beta \mathbf{v}_2^*$, where α and β are the Bloch wavenumbers. With the notation $\mathbf{x} = (x, y, z) \in \mathbb{R}^3$ and $\tilde{\mathbf{x}} = (x, y)$ and

$$r_{mn}^2 = |\tilde{\mathbf{x}} + m\mathbf{v}_1 + n\mathbf{v}_2|^2 + z^2, \tag{1}$$

the quasi-periodic Green function can be expressed in the form

$$G^{qper}(x, y, z) = \frac{1}{4\pi} \sum_{m,n \in \mathbb{Z}} \frac{e^{ikr_{mn}}}{r_{mn}} \cdot e^{-i\mathbf{k} \cdot (m\mathbf{v}_1 + n\mathbf{v}_2)}. \tag{2}$$

Notice that $\mathbf{k} \cdot (m\mathbf{v}_1 + n\mathbf{v}_2) = \alpha m + \beta n$. The function $G^{qper}(x, y, z)$ possesses the quasi-periodic property

$$G^{qper}(\tilde{\mathbf{x}} + m\mathbf{v}_1 + n\mathbf{v}_2, z) = G^{qper}(\tilde{\mathbf{x}}, z)e^{i(\alpha m + \beta n)}. \tag{3}$$

The series expansion (2) possesses notoriously poor convergence properties. Various methods to accelerate its convergence, notably the Ewald method [16, 13, 22], have been proposed. A survey in these regards is given in [18], and a comprehensive discussion of lattice summation techniques can be found in [3]. A few remarks concerning the computational costs associated with previous accelerated methods for evaluation of the Green function (2) are presented below in this section.

In the approach proposed presently, the infinite sum (2) is evaluated by multiplying its (m, n)-th term by the value $\chi_a(\tilde{r}_{mn})$ of a slow-rise smooth windowing function χ_a which, evaluated at the *cylindrical radius*

$$\tilde{r}_{mn} = |m\mathbf{v}_1 + n\mathbf{v}_2|, \tag{4}$$

restricts the sum to values of m and n satisfying $0 \le \tilde{r}_{mn} \le a$. (Note that $\tilde{r}_{mn} = r_{mn}$ if and only if $z = 0$.) The function $\chi_a = \chi_a(\tilde{r})$ is obtained as a scaled version of an infinitely smooth real valued function χ defined on the set of non-negative real numbers $\tilde{r} \ge 0$, which equals zero for $\tilde{r} > a$ and equals 1 for $0 \le \tilde{r} < c\,a$, where $c < 1$ is an adequately selected real number. (For the numerical experiments presented in this paper the value $c = 0.5$ was used.) The function χ_a is then defined by

$$\chi_a(\tilde{r}) = \chi(\tilde{r}/a); \tag{5}$$

clearly χ_a decreases from 1 to 0 in a slow manner: its derivative tends to zero as $a \to \infty$ throughout the region of decrease $c \cdot a \le \tilde{r} \le a$.

The main results in this contribution include *(i)* A proof, presented in Section 2, establishing that, as the truncation radius a tends to $+\infty$, the smoothly truncated Green function converges

faster than any negative power of a—at least for arrangements of the period, frequency and incidence angles that lie away from certain "Wood configurations" (for which the Green function G^{qper} ceases to exist); as well as *(ii)* A new accelerated integral-equation solver presented in Section 3 which, relying on the aforementioned windowed Green function, gives rise to a highly-efficient overall solution method for the problems at hand. In particular, Theorem 2.1 below establishes the super-algebraically fast convergence of the truncated sum to the three-dimensional quasi-periodic Green function away from Wood configurations; a corresponding convergence theorem for 1D-periodic diffraction gratings in $\mathbb{R}^2$ was presented in [19], cf. also [4]. Figures 1 and 2 in Section 2 demonstrate the convergence of the windowed series both near and away from Wood configurations. The numerical methods presented in Sections 3, in turn, integrate the windowed Green function in the context of fast integral-equation solvers [8, 9]. Interestingly, the structure of the acceleration methodology inherent in these solvers is exploited to completely avoid evaluation of the windowed Green function at pairs of surface points, using instead a much smaller number of values of the Green function on a certain three-dimensional Cartesian grid. A variety of numerical results presented in Section 4 demonstrate the character of the resulting solvers for bi-periodic scattering problems. Green function methods that are valid even at and around Wood configurations are presented in [4] for two-dimensional configurations, and in Part II for the three-dimensional case.

As is well known, for certain wave numbers k and certain Bloch wave numbers (α, β), the lattice sum (2) does not converge. This can be seen in the spectral representation of the Green function that results by applying the Poisson Summation Formula to the series (2). Let $d = \|\mathbf{v}_1 \times \mathbf{v}_2\|$. Then

$$G^{qper}(\tilde{\mathbf{x}}, z) = \frac{i}{2d} \sum_{j,\ell \in \mathbb{Z}} \frac{1}{\gamma_{j\ell}} e^{i[(2\pi j\,\mathbf{v}_1^* + 2\pi\ell\,\mathbf{v}_2^*) + \mathbf{k}]\cdot\tilde{\mathbf{x}}}\, e^{i\gamma_{j\ell}|z|}\,, \tag{6}$$

in which the propagation constants $\gamma_{j\ell}$ are defined by

$$\mathbf{v}_{j\ell}^* = (2\pi j\,\mathbf{v}_1^* + 2\pi\ell\,\mathbf{v}_2^*) + \mathbf{k}\,, \quad \gamma_{j\ell} = (k^2 - \|\mathbf{v}_{j\ell}^*\|^2)^{\frac{1}{2}}\,. \tag{7}$$

(The branch of the square root that defines $\gamma_{j\ell}$ is selected in such a way that $\sqrt{1} = 1$, and that the branch cut coincides with the negative imaginary semiaxis.) The lattice sum (2) converges if and only if $\gamma_{j\ell} \neq 0$ for all integer pairs (j, ℓ). Configurations for which $\gamma_{j\ell}$ vanishes for one or more integer pairs (j, ℓ) are known as Wood configurations, or Wood anomalies. Clearly the expression (6) is not meaningful if $\gamma_{j\ell} = 0$ for some integer pair (j, ℓ). Wood anomalies were first noticed by Wood [26] and first treated mathematically by Rayleigh [23]; a brief discussion concerning historical aspects in these regards can be found in [4, Remark 2.2]. As shown in [4] and Part II, Green function methods can still be used at Wood anomalies provided appropriately defined Green functions are used.

In view of the branch used in equation (7) for the square root function, Rayleigh waves either decay as $|z|$ increases (evanescent modes) or are outgoing traveling waves (propagating modes). Clearly, there exist finitely many propagating modes for any given configuration. Wood frequencies are also called "cutoff frequencies", since the corresponding Rayleigh wave $e^{i\mathbf{v}_{j\ell}^*\cdot\tilde{\mathbf{x}}} e^{i\gamma_{j\ell}|z|}$ switches from propagating to evanescent as the frequency descends below a Wood value. Rayleigh waves for which $\gamma_{j\ell}$ is small impinge on the periodic structure at "grazing incidence", and they dominate the sum (6). In the limit of a particular combination of k and (α, β), at which one or more $\gamma_{j\ell}$ are zero, the product of the sum multiplied by any one of the vanishing $\gamma_{j\ell}$'s tends to a z-independent linear combination of exactly grazing waves of the form $e^{i\mathbf{v}_{j\ell}^*\cdot\tilde{\mathbf{x}}}$.

Challenges in the calculation of the Green function arise from two main sources, namely

1. The lattice sum (2) does not converge absolutely. This sum does converge conditionally away from Wood anomalies [10], but its convergence, which results from cancellations amongst slowly decreasing terms, is too slow to be useful from a computational standpoint.

2. At Wood configurations the lattice sum (2) does not converge and a denominator in the Rayleigh-wave expansion (6) exactly vanishes. Additionally, the convergence of the series (2) increasingly deteriorates as the parameters in the problem are varied in such a way that a Wood configuration is approached.

The first of these challenges is addressed in the present contribution, and the second is treated in [4] for the two-dimensional case, and, for three dimensions, in Part II [11].

As mentioned above, the proposed approach for summation of the series is based on smooth windowing of the series (2). A similar windowed-summation technique can be applied to the spectral series (6) with similar super-algebraic convergence. A study of the potential advantages offered by such a strategy is left for future work.

Previous accelerated procedures based on either or both of the spatial and spectral representations for the Green function G^{qper} give rise to significantly faster algorithms than does direct summation of either the expressions (2) or (6). The two-dimensional algorithms (see e.g. [20, Section 3.8.2]) and [25]) can be perfectly adequate, but in the three-dimensional context algorithms for evaluation of quasi-periodic Green functions have remained inefficient. As a significant reference in these regards we mention one of the most advanced hybrid approaches previously put forth for evaluation of periodic Green's functions [17], which is based on use of a combination of spatial and spectral representations as well as Kummer and Shanks transforms. The hybrid algorithm [17] has been reported [2] (cf. also [17]) to require several milliseconds per evaluation point. Thus, even for a small discretization consisting of $N = 6 \times 16 \times 16$ points (assuming a total of 6 patches are used to represent a given scattering surface S, and 6×6 discretization points are used in each patch) the number 2×10^6 of evaluations of periodic Green functions which are necessary to evaluate one matrix-vector product requires a computational time of at least 2×10^3 seconds. In contrast, as it can be seen in Table 2, in the case of periodic two-dimensional arrays of spheres discretized by means of such a $6 \times 16 \times 16$ mesh, our solvers require less than 10 seconds per matrix-vector product (an improvement factor of a least one-hundred)—and can produce full scattering results with an error of the order of 10^{-4} in a total of 55 seconds.

As mentioned above, boundary-integral equations based on the proposed Green-function methods are presented in Section 3. In particular, Section 3 describes the numerical methods used to implement the proposed fast lattice sums and forward maps (matrix-vector products) which, upon use of an iterative linear algebra solver (GMRES) produces the densities in certain boundary-integral representations of the scattered field. For definiteness, in all numerical examples it was assumed the scatterers satisfy sound-soft (Dirichlet) boundary conditions. Section 4 demonstrates the resulting method by means of a variety of numerical results. A few concluding remarks are presented in Section 5.

2 Proof of fast convergence of smoothly truncated lattice sums

Our smooth truncation method proceeds by multiplying the (m, n)-th term of the series (2) by the scaled cut-off function $\chi(\tilde{r}_{mn}/a)$ defined in equation (5); the smoothly truncated series is thus

given by the finite sum

$$G^a(x,y,z) := \frac{1}{4\pi} \sum_{m,n\in\mathbb{Z}} \frac{e^{ikr_{mn}}}{r_{mn}} e^{-i\mathbf{k}\cdot(m\mathbf{v}_1+n\mathbf{v}_2)} \chi(\tilde{r}_{mn}/a) \approx G^{qper}(x,y,z), \tag{8}$$

where of r_{mn} and $\tilde{r}_{mn}$ are given by (1) and (4). The following theorem establishes the super-algebraic convergence of the truncated lattice sum to the quasi-periodic Green function for configurations away from Wood anomalies.

Theorem 2.1 (Windowed Green function at non-Wood frequencies: Super-algebraic convergence).
Let $\chi(r)$ be an infinitely smooth truncation function which equals to 1 for $r \le r_1$ and equals 0 for $r \ge r_2$ $(0 < r_1 < r_2)$. If $\gamma_{j\ell} \ne 0$ for all $(j,\ell) \in \mathbb{Z}^2$, then the functions

$$G^a(x,y,z) = \frac{1}{4\pi} \sum_{m,n\in\mathbb{Z}} \frac{e^{ikr_{mn}}}{r_{mn}} e^{-i\mathbf{k}\cdot(m\mathbf{v}_1+n\mathbf{v}_2)} \chi(\tilde{r}_{mn}/a)$$

converge to the radiating quasi-periodic Green function $G^{qper}(x,y,z)$ super-algebraically fast as the truncation radius a tends to infinity. In detail, for each positive integer n there exist constants $C_n = C_n(k,\alpha,\beta)$ such that

$$|G_k^a(x,y,z) - G^{qper}(x,y,z)| < \frac{C_n(k,\alpha,\beta)}{a^n} \tag{9}$$

when a is sufficiently large. The inequality holds uniformly for all points (x,y,z), excluding the singularities of the Green function for which $r_{mn} = 0$ for some $(m,n) \in \mathbb{Z}^2$. At these points, a term that is common to G_k^a and G^{qper} is infinite. If G_k^a and G^{qper} are modified by excluding this term then the correspondingly modified version of equation (9) remains valid.
An analogous estimate holds for $\|\nabla G_k^a(x,y,z) - \nabla G^{qper}(x,y,z)\|$.

Proof. Denote by $\Lambda = \{m\mathbf{v}_1 + n\mathbf{v}_2 : m,n \in \mathbb{Z}\}$ the lattice of singularities of the Green function, and denote by $\Lambda^* = \{j\mathbf{v}_1^* + \ell\mathbf{v}_2^* : j,\ell \in \mathbb{Z}\}$ the dual lattice. The dual vectors $\mathbf{v}_1^*$ and $\mathbf{v}_2^*$ are defined by $\mathbf{v}_i^* \cdot \mathbf{v}_j = \delta_{ij}$. Initially, we assume that the shift $\tilde{\mathbf{x}} = (x,y)$ from these positions as well as the Bloch wavenumbers α and β are equal to zero. Setting $\varepsilon = a^{-1}$, we have for the full and the truncated sums,

$$4\pi G^{qper} = \sum_{\mathbf{r}\in\Lambda} \frac{\exp(ik\sqrt{|\mathbf{r}|^2 + z^2})}{\sqrt{|\mathbf{r}|^2 + z^2}} \tag{10}$$

and

$$4\pi G^a = \sum_{\mathbf{r}\in\Lambda} \chi(\varepsilon|\mathbf{r}|) \frac{\exp(ik\sqrt{|\mathbf{r}|^2 + z^2})}{\sqrt{|\mathbf{r}|^2 + z^2}} . \tag{11}$$

With the view of utilizing the Poisson summation formula to calculate the truncated sum we introduce a smooth function $\phi(|\mathbf{r}|)$ that vanishes in a neighborhood of $|\mathbf{r}| = 0$ and is equal to 1 for $|\mathbf{r}| \ge r_1$. For $\varepsilon < 1$, the sum is broken into two pieces,

$$\sum_{\mathbf{r}\in\Lambda} \chi(\varepsilon|\mathbf{r}|) \frac{\exp(ik\sqrt{|\mathbf{r}|^2 + z^2})}{\sqrt{|\mathbf{r}|^2 + z^2}}$$

$$= \sum_{0\ne\mathbf{r}\in\Lambda} (1 - \phi(|\mathbf{r}|)) \frac{\exp(ik\sqrt{|\mathbf{r}|^2 + z^2})}{\sqrt{|\mathbf{r}|^2 + z^2}} + \sum_{\mathbf{r}\in\Lambda} \phi(|\mathbf{r}|)\chi(\varepsilon|\mathbf{r}|) \frac{\exp(ik\sqrt{|\mathbf{r}|^2 + z^2})}{\sqrt{|\mathbf{r}|^2 + z^2}} . \tag{12}$$

5

In the first sum on the right, χ is omitted as a factor since it equals unity when $\phi \neq 1$. The term is thus independent of the truncation variable ε. It is easy to check that the fraction in the second term can be expressed as a product of an exponential function and a Laurent expansion:

$$\frac{\exp(ik\sqrt{r^2+z^2})}{\sqrt{r^2+z^2}} = \frac{e^{ikr}}{r}g(r), \qquad g(r) = 1 + \sum_{j=1}^{\infty} a_j r^{-j}. \tag{13}$$

The coefficients a_j are functions of z and the expansion is convergent when $r > |z|$.

We re-express the second sum in (12) by means of the Poisson summation formula:

$$\sum_{\boldsymbol{r}\in\Lambda} \phi(|\boldsymbol{r}|)\chi(\varepsilon|\boldsymbol{r}|)g(|\boldsymbol{r}|)\frac{e^{ik|\boldsymbol{r}|}}{|\boldsymbol{r}|} = \frac{1}{d}\sum_{\boldsymbol{\xi}\in\Lambda^*} \mathcal{F}\left[\phi(|\boldsymbol{r}|)\chi(\varepsilon|\boldsymbol{r}|)g(|\boldsymbol{r}|)\frac{e^{ik|\boldsymbol{r}|}}{|\boldsymbol{r}|}\right](\boldsymbol{\xi}), \tag{14}$$

where $d = \|\mathbf{v}_1 \times \mathbf{v}_2\|$. In what follows we re-express the Fourier transform on the right-hand side of this equation (which, for brevity, we denote by $\mathcal{F}(\boldsymbol{\xi})$) in terms of suitable contour integrals. To do this, we represent the spatial and Fourier variables in polar coordinates, $\boldsymbol{r} = (r, \theta)$ and $\boldsymbol{\xi} = (\xi, \gamma)$, and we let $f(r) = \phi(r)g(r)$, and we thus obtain

$$\mathcal{F}(\boldsymbol{\xi}) = \int_0^\infty \int_{-\pi}^\pi f(r)\chi(\varepsilon r)e^{i(k-2\pi\xi\cos(\theta-\gamma))r}d\theta dr$$

$$= 2\int_0^\infty f(r)\chi(\varepsilon r)\int_0^\pi e^{i(k-2\pi\xi\cos\theta)r}d\theta dr = 2\int_0^\infty f(r)\chi(\varepsilon r)\int_{-1}^1 e^{i(k-2\pi\xi s)r}\frac{ds}{\sqrt{1-s^2}}dr$$

$$= 2\int_0^\infty f(r)\chi(\varepsilon r)\left(\int_{-1}^{-1-i\infty} e^{i(k-2\pi\xi s)r}\frac{ds}{\sqrt{1-s^2}}dr - \int_1^{1-i\infty} e^{i(k-2\pi\xi s)r}\frac{ds}{\sqrt{1-s^2}}dr\right). \tag{15}$$

The last equality is valid by contour integration in the complex s-plane in view of the exponential decay of the integrand as $\mathrm{Im}(s) \to -\infty$. We have thus obtained

$$\mathcal{F}(\boldsymbol{\xi}) = 2\left(\int_{-1}^{-1-i\infty} I(s)\frac{ds}{\sqrt{1-s^2}} - \int_1^{1-i\infty} I(s)\frac{ds}{\sqrt{1-s^2}}\right) \tag{16}$$

where

$$I(s) = \int_0^\infty f(r)\chi(\varepsilon r)e^{i(k-2\pi\xi s)r}dr. \tag{17}$$

The integrand (17) decays exponentially fast at infinity since $\mathrm{Im}(s) < 0$. Thus, integration by parts (in which the boundary terms vanish because $f(r)$ vanishes near $r = 0$) yields

$$I(s) = \frac{1}{i(k-2\pi\xi s)}\int_0^\infty \left[f'(r) + f'(r)(\chi(\varepsilon r)-1) + \varepsilon f(r)\chi'(\varepsilon r)\right]e^{i(k-2\pi\xi s)r}dr$$

$$= I_0(s) + I_\varepsilon(s) \tag{18}$$

where

$$I_0(s) = \frac{1}{i(k-2\pi\xi s)}\int_0^\infty f'(r)e^{i(k-2\pi\xi s)r}dr = \frac{1}{[i(k-2\pi\xi s)]^n}\int_0^\infty f^{(n)}(r)e^{i(k-2\pi\xi s)r}dr, \tag{19}$$

6

and where, noting that $\{\chi = 1\} \supseteq \{\phi \neq 1\}$ for $\varepsilon < 1$, we have $\chi - 1 = 0$, $\chi' = 0$ and $f(r) = g(r)$ in the region $\{\chi = 1\}$, and, thus

$$I_\varepsilon(s) = \frac{1}{i(k - 2\pi\xi s)} \int_0^\infty \left[g'(r)(\chi(\varepsilon r) - 1) + \varepsilon g(r)\chi'(\varepsilon r) \right] e^{i(k-2\pi\xi s)r} dr. \tag{20}$$

Thus, introducing a rescaled version g_ε of the function g,

$$g_\varepsilon(\rho) = g(\rho/\varepsilon) = \frac{\rho}{\sqrt{\rho^2 + (\varepsilon z)^2}} \exp\left(\frac{ikz^2\varepsilon}{\rho + \sqrt{\rho^2 + (\varepsilon z)^2}} \right) = 1 + \sum_{j=1}^\infty a_j \frac{\varepsilon^j}{\rho^j} \tag{21}$$

the integrals $I_\varepsilon(s)$ become

$$\begin{aligned}
I_\varepsilon(s) &= \frac{\varepsilon}{i(k - 2\pi\xi s)} \int_0^\infty \left[g_\varepsilon'(\varepsilon r)(\chi(\varepsilon r) - 1) + g_\varepsilon(\varepsilon r)\chi'(\varepsilon r) \right] e^{i(k-2\pi\xi s)r} dr \\
&= \frac{1}{i(k - 2\pi\xi s)} \int_0^\infty \left[g_\varepsilon'(\rho)(\chi(\rho) - 1) + g_\varepsilon(\rho)\chi'(\rho) \right] e^{i(k-2\pi\xi s)\rho/\varepsilon} d\rho \\
&= \frac{(-1)^n \varepsilon^n}{[i(k - 2\pi\xi s)]^{n+1}} \int_0^\infty \frac{d^n}{d\rho^n} \left[g_\varepsilon'(\rho)(\chi(\rho) - 1) + g_\varepsilon(\rho)\chi'(\rho) \right] e^{i(k-2\pi\xi s)\rho/\varepsilon} d\rho.
\end{aligned}$$

In view of (16), the splitting $I(s) = I_0(s) + I_\varepsilon(s)$ effects the splitting

$$\mathcal{F}(\boldsymbol{\xi}) = \mathcal{F}_0(\boldsymbol{\xi}) + \mathcal{F}_\varepsilon(\boldsymbol{\xi}), \tag{22}$$

for $\mathcal{F}(\boldsymbol{\xi})$, where letting

$$S_\pm(\rho) = \int_{\pm 1}^{\pm 1 - i\infty} \frac{e^{i(k-2\pi\xi s)\rho/\varepsilon}}{[i(k - 2\pi\xi s)]^{n+1}} \frac{ds}{\sqrt{1 - s^2}} = -2i \int_0^\infty \frac{e^{(i(k\mp 2\pi\xi) - 2\pi\xi t^2)\rho/\varepsilon}}{[i(k \mp 2\pi\xi) - 2\pi\xi t^2]^{n+1}} \frac{dt}{\sqrt{\pm 2i + t^2}} \tag{23}$$

(the last expression of which incorporates the changes of variables $s = \pm 1 - it^2$) we have denoted

$$\mathcal{F}_0(\boldsymbol{\xi}) = 2 \int_0^\infty f^{(n)}(r) \left(\int_{-1}^{-1-i\infty} \frac{e^{i(k-2\pi\xi s)r}}{[i(k - 2\pi\xi s)]^n} \frac{ds}{\sqrt{1 - s^2}} dr - \int_1^{1-i\infty} \frac{e^{i(k-2\pi\xi s)r}}{[i(k - 2\pi\xi s)]^n} \frac{ds}{\sqrt{1 - s^2}} dr \right) \tag{24}$$

and

$$\mathcal{F}_\varepsilon(\boldsymbol{\xi}) = 2(-1)^n \varepsilon^n \int_0^\infty \frac{d^n}{d\rho^n} \left[g_\varepsilon'(\rho)(\chi(\rho) - 1) + g_\varepsilon(\rho)\chi'(\rho) \right] (S_-(\rho) - S_+(\rho)) \, d\rho. \tag{25}$$

Assume now that $\xi \neq 0$; the case $\xi = 0$ will be treated separately. In view of the hypothesis $k - 2\pi\xi \neq 0$ the integral $|S_+|$ admits the finite upper bound

$$\begin{aligned}
|S_+(\rho)| &\leq \int_0^\infty \frac{2 \, e^{-2\pi\xi t^2 \rho/\varepsilon} dt}{[(k - 2\pi\xi)^2 + (2\pi\xi t^2)^2]^{\frac{n+1}{2}} (4 + t^4)^{\frac{1}{4}}} \leq \int_0^\infty \frac{\sqrt{2} \, e^{-2\pi\xi t^2 \rho/\varepsilon} dt}{|k - 2\pi\xi|^{n+1}} \tag{26} \\
&= \left(\frac{\varepsilon}{\rho\xi} \right)^{\frac{1}{2}} \frac{1}{|k - 2\pi\xi|^{n+1}} \int_0^\infty e^{-\pi t^2} dt = \frac{1}{2} \left(\frac{\varepsilon}{\rho\xi} \right)^{\frac{1}{2}} \frac{1}{|k - 2\pi\xi|^{n+1}}. \tag{27}
\end{aligned}$$

Analogously, in view of the assumption $k + 2\pi\xi \neq 0$ we obtain

$$|S_-(\rho)| \leq \frac{1}{2} \left(\frac{\varepsilon}{\rho\xi} \right)^{\frac{1}{2}} \frac{1}{|k + 2\pi\xi|^{n+1}}. \tag{28}$$
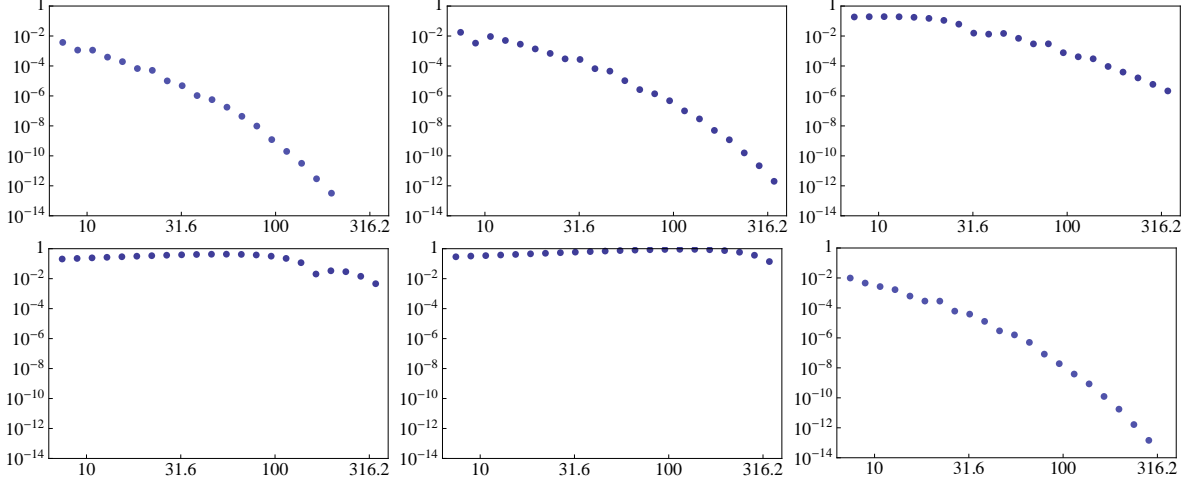
7

Figure 1: The error in the approximation of the quasi-periodic Green function by multiplying the lattice sum by a smooth truncation function $\chi((m+x)/a)\chi((n+y)/a)$, in which $\chi(s) = \exp(2e^{1/(1-x)}/(x-2))$. The plots show $\max_{(x,y,z)\in K} |G_{i+1} - G_i|$ as a function of a_i on a *log-log* scale, in which a truncated lattice sum G_i is computed for $a = a_i = 1.2^i$, $\hat{\mathbf{x}} = (\hat{x},\hat{y},\hat{z}) = (0,0,1)$ and (x,y,z) on a grid K of evenly spaced points in $[0,0.6]\times[0,0.6]\times[0.6,1.4]$, excluding $\hat{\mathbf{x}} = \mathbf{x}$. The lattice vectors are $\mathbf{v}_1 = (1,0,0)$ and $\mathbf{v}_2 = (0,1,0)$, the Bloch wavevector is $(\kappa_1 = 0, \kappa_2 = 0)$, and the frequencies are $k = 0.4, 0.8, 0.95$ (first row) and $k = 0.99, 2.24, 2.5$ (second row). Both $k = 1.0$ and $k \approx 2.23607$ are Wood frequencies, at which convergence is not available.

Returning to the expression for $\mathcal{F}_\varepsilon(\boldsymbol{\xi})$ above, observe that, since $\chi(\rho) = 1$ for $\rho \le r_1$, and $\chi(\rho) = 0$ for $\rho \ge r_2$, the integral in ρ from 0 to ∞ in (25) can be re-expressed in the form $\mathcal{F}_\varepsilon(\boldsymbol{\xi}) = \mathcal{F}_\varepsilon^1(\boldsymbol{\xi}) + \mathcal{F}_\varepsilon^2(\boldsymbol{\xi})$ where

$$\mathcal{F}_\varepsilon^1(\boldsymbol{\xi}) = 2(-1)^n \varepsilon^n \int_{r_1}^{r_2} \frac{d^n}{d\rho^n}\left[g_\varepsilon'(\rho)(\chi(\rho) - 1) + g_\varepsilon(\rho)\chi'(\rho)\right]\left(S_-(\rho) - S_+(\rho)\right) d\rho \quad \text{and}$$

$$\mathcal{F}_\varepsilon^2(\boldsymbol{\xi}) = 2(-1)^{n+1}\varepsilon^n \int_{r_2}^{\infty} g_\varepsilon^{(n+1)}(\rho)\left(S_-(\rho) - S_+(\rho)\right) d\rho\,.$$

The bounds (26) and (28) thus imply

$$\left|\mathcal{F}_\varepsilon^1(\boldsymbol{\xi})\right| \le \frac{\varepsilon^{n+\frac{1}{2}}}{\xi^{\frac{1}{2}}}\left(\frac{1}{|k - 2\pi\xi|^{n+1}} + \frac{1}{|k + 2\pi\xi|^{n+1}}\right)\int_{r_1}^{r_2}\left|\frac{d^n}{d\rho^n}\left[g_\varepsilon'(\rho)(\chi(\rho) - 1) + g_\varepsilon(\rho)\chi'(\rho)\right]\right|\frac{d\rho}{\rho^{\frac{1}{2}}}\,. \tag{29}$$

Clearly, as $\varepsilon \to 0$ the functions $g_\varepsilon(\rho)$ converge to 1 uniformly over the interval $[r_1, r_2]$, and thus the integral (29) integral converges to $\int_{r_1}^{r_2} \chi^{(n+1)}(\rho)\rho^{-1/2}d\rho$ in this limit. In particular these integrals are bounded by a constant $C_n^1 > 0$ for all $\varepsilon < 1$ and we have

$$\left|\mathcal{F}_\varepsilon^1(\boldsymbol{\xi})\right| \le C_n^1 \frac{\varepsilon^{n+\frac{1}{2}}}{\xi^{\frac{1}{2}}}\left(\frac{1}{|k - 2\pi\xi|^{n+1}} + \frac{1}{|k + 2\pi\xi|^{n+1}}\right). \tag{30}$$

Similarly, for $\mathcal{F}_\varepsilon^2(\boldsymbol{\xi})$ we have

$$\left|\mathcal{F}_\varepsilon^2(\boldsymbol{\xi})\right| \le \frac{\varepsilon^{n+\frac{1}{2}}}{\xi^{\frac{1}{2}}}\left(\frac{1}{|k - 2\pi\xi|^{n+1}} + \frac{1}{|k + 2\pi\xi|^{n+1}}\right)\int_{r_2}^{\infty}\left|g_\varepsilon^{(n+1)}(\rho)\right|\frac{d\rho}{\rho^{\frac{1}{2}}}\,. \tag{31}$$
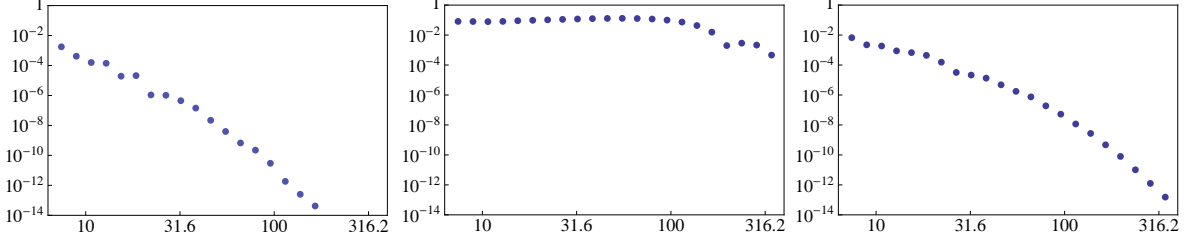
8

Figure 2: These plots are similar to those in Fig. 1 except that the Bloch wavevector is $(\kappa_1 = 0.4, \kappa_2 = -0.3)$, and the frequencies are $k = 0.3, 0.93, 1.1$. There is a Wood frequency at $k \approx 0.921954$.

But from (21) we obtain

$$
g_\varepsilon^{(n+1)}(\rho) = \frac{(-1)^{n+1}}{\rho^{n+1}} \sum_{j=1}^\infty a_j \frac{(j+n)!}{(j_1)!} \frac{\varepsilon^j}{\rho^j}, \tag{32}
$$

and, we thus see that, for ε sufficiently small, $\int_{r_2}^\infty \left| g_\varepsilon^{(n+1)}(\rho) \right| \rho^{-\frac{1}{2}} d\rho$ is bounded by a certain constant C_n^2, so that

$$
\left| \mathcal{F}_\varepsilon^2(\xi) \right| \le C_n^2 \frac{\varepsilon^{n+\frac{1}{2}}}{\xi^{\frac{1}{2}}} \left(\frac{1}{|k - 2\pi\xi|^{n+1}} + \frac{1}{|k + 2\pi\xi|^{n+1}} \right). \tag{33}
$$

Combining the estimates $\mathcal{F}_\varepsilon^1(\xi)$ and $\mathcal{F}_\varepsilon^2(\xi)$ we thus find that there exists a constant C_n^3 such that

$$
|\mathcal{F}_\varepsilon(\xi)| \le \varepsilon^{n+\frac{1}{2}} \frac{C_n^3}{\xi^{\frac{1}{2}}} \left(\frac{1}{|k - 2\pi\xi|^{n+1}} + \frac{1}{|k + 2\pi\xi|^{n+1}} \right). \tag{34}
$$

For $\xi = 0$, in turn, we have

$$
\mathcal{F}(\mathbf{0}) = \int_0^\infty \int_{-\pi}^\pi f(r)\chi(\varepsilon r)e^{ikr} d\theta dr = 2\pi \int_0^\infty f(r)\chi(\varepsilon r)e^{ikr} dr =
$$

$$
= -\frac{2\pi}{ik} \int_0^\infty f'(r)e^{ikr} dr - \frac{2\pi}{ik} \int_0^\infty \left[g_\varepsilon'(\rho)(\chi(\rho) - 1) + g_\varepsilon(\rho)\chi'(\rho) \right] e^{ik\rho/\varepsilon} d\rho
$$

$$
= -\frac{2\pi}{ik} \int_0^\infty f'(r)e^{ikr} dr + (-1)^n \frac{2\pi}{ik} \left(\frac{\varepsilon}{ik} \right)^{n+1} \int_0^\infty \frac{d^n}{d\rho^n} \left[g_\varepsilon'(\rho)(\chi(\rho) - 1) + g_\varepsilon(\rho)\chi'(\rho) \right] e^{ik\rho/\varepsilon} d\rho
$$

$$
= \mathcal{F}_0(\mathbf{0}) + \mathcal{F}_\varepsilon(\mathbf{0}). \tag{35}
$$

Again, $\mathcal{F}_0(\mathbf{0})$ is independent of ε and the integral in $\mathcal{F}_\varepsilon(\mathbf{0})$ has a limit as $\varepsilon \to 0$. Thus one obtains constants $C_n^0 > 0$ such that $|\mathcal{F}_\varepsilon(\mathbf{0})| \le C_n^0 \varepsilon^{n+1}$.

The estimates above now allow us to now establish the convergence as $\varepsilon \to 0$ of the series on the right-hand side of equation (14). If $n \ge 1$, then as long as $2\pi|\xi| \ne |k|$ for all $\xi \in \Lambda^*$, the sum of $|\mathcal{F}_\varepsilon(\xi)|$ over all $\xi \in \Lambda^*$ is convergent, and one obtains

$$
\sum_{\xi \in \Lambda^*} |\mathcal{F}_\varepsilon(\xi)| \le C_n \varepsilon^{n+\frac{1}{2}}. \tag{36}
$$

The Poisson Summation Formula now gives

$$
d \sum_{\mathbf{r} \in \Lambda} \phi(|\mathbf{r}|)\chi(\varepsilon|\mathbf{r}|)g(|\mathbf{r}|) \frac{e^{ik|\mathbf{r}|}}{|\mathbf{r}|} = \sum_{\xi \in \Lambda^*} \mathcal{F}_0(\xi) + \sum_{\xi \in \Lambda^*} \mathcal{F}_\varepsilon(\xi). \tag{37}
$$

9

But the first term on the right hand side of this equation is independent of ε, and, in view of (36), the second term on the right hand side tends to zero super-algebraically fast. It follows that the sum on the left hand side of (37) converges super-algebraically fast, as needed.

Inclusion of the Bloch quasi-periodicity factors in the lattice sum can now be accomplished by replacing the expression $\exp(ik\sqrt{|\boldsymbol{r}|^2 + z^2})/\sqrt{|\boldsymbol{r}|^2 + z^2}$ by

$$\frac{\exp(ik\sqrt{|\boldsymbol{r}|^2 + z^2})}{\sqrt{|\boldsymbol{r}|^2 + z^2}} e^{-i\mathbf{k}\cdot\boldsymbol{r}}, \tag{38}$$

where $\mathbf{k} = \alpha\mathbf{v}_1^* + \beta\mathbf{v}_2^*$. Equation (37) becomes

$$d \sum_{\boldsymbol{r}\in\Lambda} \phi(|\boldsymbol{r}|)\chi(\varepsilon|\boldsymbol{r}|)g(|\boldsymbol{r}|)\frac{e^{ik|\boldsymbol{r}|}}{|\boldsymbol{r}|}e^{-i\mathbf{k}\cdot\boldsymbol{r}} = \sum_{\boldsymbol{\xi}\in\Lambda^*} \mathcal{F}_0\left(\boldsymbol{\xi} + \frac{\mathbf{k}}{2\pi}\right) + \sum_{\boldsymbol{\xi}\in\Lambda^*} \mathcal{F}_\varepsilon\left(\boldsymbol{\xi} + \frac{\mathbf{k}}{2\pi}\right), \tag{39}$$

The bound (34), shifted by $\mathbf{k}/2\pi$, is

$$\left|\mathcal{F}_\varepsilon\left(\boldsymbol{\xi} + \frac{\mathbf{k}}{2\pi}\right)\right| \le \varepsilon^{n+\frac{1}{2}}\frac{C_n^3}{\xi^{\frac{1}{2}}}\left(\frac{1}{\left|k - 2\pi\left|\boldsymbol{\xi} + \mathbf{k}/(2\pi)\right|\right|^{n+1}} + \frac{1}{\left|k + 2\pi\left|\boldsymbol{\xi} + \mathbf{k}/(2\pi)\right|\right|^{n+1}}\right),$$

which is valid whenever

$$k^2 \ne |2\pi\boldsymbol{\xi} + \mathbf{k}|^2. \tag{40}$$

The validity of (40) for all $\xi \in \mathbb{Z}^2$ is exactly the condition that (k, α, β) is not a Wood triple.

Inclusion of a shift in $\boldsymbol{r}$ by a fixed vector $\boldsymbol{r}' = (x, y)$. Consider the lattice sum of the quantities

$$\frac{\exp(ik\sqrt{|\boldsymbol{r} - \boldsymbol{r}'|^2 + z^2})}{\sqrt{|\boldsymbol{r} - \boldsymbol{r}'|^2 + z^2}}, \tag{41}$$

in which we have taken $\mathbf{k} = 0$. The case $\mathbf{k} \ne 0$ is again treated by shifting the Fourier variable $\boldsymbol{\xi}$ as shown above. As the cutoff functions ϕ and χ are also shifted, there ensues a mere exponential factor in the Fourier transform, and equation (37) becomes

$$d \sum_{\boldsymbol{r}\in\Lambda} \phi(|\boldsymbol{r} - \boldsymbol{r}'|)\chi(\varepsilon|\boldsymbol{r} - \boldsymbol{r}'|)g(|\boldsymbol{r} - \boldsymbol{r}'|)\frac{e^{ik|\boldsymbol{r}-\boldsymbol{r}'|}}{|\boldsymbol{r} - \boldsymbol{r}'|} = \sum_{\boldsymbol{\xi}\in\Lambda^*} \mathcal{F}_0(\boldsymbol{\xi})e^{-2\pi i\boldsymbol{\xi}\cdot\boldsymbol{r}'} + \sum_{\boldsymbol{\xi}\in\Lambda^*} \mathcal{F}_\varepsilon(\boldsymbol{\xi})e^{-2\pi i\boldsymbol{\xi}\cdot\boldsymbol{r}'}. \tag{42}$$

The bound (36) persists,

$$\left|\sum_{\boldsymbol{\xi}\in\Lambda^*} \mathcal{F}_\varepsilon(\boldsymbol{\xi})e^{-2\pi i\boldsymbol{\xi}\cdot\boldsymbol{r}'}\right| \le C_n\,\varepsilon^{n+\frac{1}{2}}, \tag{43}$$

and one again obtains super-algebraic convergence.

Error bound for the gradient of the Green function. The gradient of the monopole e^{ikr}/r is given by the equations

$$\frac{\partial}{\partial x}\frac{e^{ikr}}{r} = \left(ik\cos\theta - \frac{\cos\theta}{r}\right)\frac{e^{ikr}}{r}, \qquad \frac{\partial}{\partial y}\frac{e^{ikr}}{r} = \left(ik\sin\theta - \frac{\sin\theta}{r}\right)\frac{e^{ikr}}{r}. \tag{44}$$

$$\frac{\partial}{\partial z}\frac{e^{ikr}}{r} = \left(ik\frac{z}{r} - \frac{z}{r^2}\right)\frac{e^{ikr}}{r}. \tag{45}$$

10

It suffices to show that the error bound proven in the theorem remains true, if the monopole $\frac{e^{ikr}}{r}$ is replaced in the proof by any of the terms of the above equations. These terms are products of the monopole multiplied by r^{-1}, or by $\cos\theta$, or by $\sin\theta$, or by a selection of two of these factors. The bound is clearly preserved when multiplying the monopole by z, since the latter factors out of the summation that constitutes the Green function.

Multiplying the monopole by r^{-1} or by r^{-2} corresponds to introducing the factor ε/ρ or $(\varepsilon/\rho)^2$ respectively in the subsequent integration over ρ, thus enhancing the error bound by one or two orders in ε. The integrand is zero (see explanation following (25)) when $\rho < r_1$, thus the denominator ρ is no cause of concern.

The following observations show that the error bound is preserved in the terms in which the monopole is multiplied by $\cos\theta$ or by $\sin\theta$.

- The first double integral of (15) acquires the factors $\cos\theta$ or $\sin\theta$ in its integrand. Thus, the second double integral in (15) (obtained by the change of the integration variable $\theta \to \theta + \gamma$) exhibits the factors $\cos(\theta + \gamma)$ or $\sin(\theta + \gamma)$ that can be split into a linear combination of $\cos\theta$ and $\sin\theta$, with the corresponding splitting of the integral.

- The double integral that contains the factor $\sin\theta$ is equal to zero; the integrand of the integration with respect to θ is an exact derivative and the integration is over the closed loop from $-\pi$ to π.

- What is left is the second double integral in (15) with the extra factor $\cos\theta$ in the integrand. The change of the variable of integration $\cos\theta = s$ leads to having an extra factor s in the subsequent integrals with respect to s. This introduces the extra factor $|s| = |\pm 1 - it^2|$ into the numerator of the first integral in (26).

- Following the change of variable $s = \pm 1 - it^2$, the factor $|s|$ is replaced by its upper bound $1 + t^2$ and the integral is split accordingly into a sum of two integrals. The first integral is exactly the one that provides the error bound of the theorem. The extra factor t^2 in the second integral provides the extra factor $\frac{\varepsilon}{\xi\rho}$ in the bounds (26) and (28) when $\xi \neq 0$. Thus, the error bound of the theorem is preserved in this case.

- If $\xi = 0$, the first integral in (35) has the factor $\cos\theta$ or $\sin\theta$ that integrates to zero.

■

3 Fast high-order integral solvers for problems of scattering by doubly-periodic structures

For definiteness we restrict our treatment to diffractive structures consisting of arrays of separated obstacles arranged in a two-dimensional periodic fashion in three-dimensional space. Thus, denoting by $\Omega \subset \mathbb{R}^3$ an open connected set the region occupied by a "reference obstacle" (which could itself be given by the union of a number of connected components) and letting $S = \partial\Omega$ denote its boundary (the reference scattering boundary), the overall three-dimensional bi-periodic scattering structure and its boundary are given by

$$\Omega_{per} = \bigcup_{(m,n)\in\mathbb{Z}\times\mathbb{Z}} \Omega_{m,n}, \quad S_{per} = \bigcup_{(m,n)\in\mathbb{Z}\times\mathbb{Z}} S_{m,n}, \tag{46}$$

11

respectively, where, we have set $\Omega_{m,n} = \Omega - m\mathbf{v}_1 - n\mathbf{v}_2$ and $S_{m,n} = S - m\mathbf{v}_1 - n\mathbf{v}_2$, $m, n \in \mathbb{Z}$. It will be assumed now that the sets $\Omega_{m,n}$, as well as their boundaries, are pairwise disjoint. Consider the sound-soft scattering problem

$$
\begin{aligned}
\Delta u + k^2 u &= 0 \text{ in } \mathbb{R}^3 \setminus \Omega_{per} \\
u &= -u^{inc} \text{ on } \partial\Omega_{per},
\end{aligned}
\tag{47}
$$

in which an incident plane wave

$$
u^{inc}(\mathbf{x}) = \exp(ik\mathbf{d} \cdot \mathbf{x}) = \exp[i(\mathbf{k} \cdot \tilde{\mathbf{x}} - \gamma z)],
\tag{48}
$$

with $|\mathbf{k}|^2 + \gamma^2 = k^2$, illuminates the structure from above and thus gives rise to a scattered field u. Owing to the periodicity of the domain Ω_{per}, in the regions Ω_+ and Ω_- above and below the array ($\Omega_+ = \{\mathbf{x} : z > \max z', (x', y', z') \in \Omega_{per}\}$, and $\Omega_- = \{\mathbf{x} : z < \min z', (x', y', z') \in \Omega_{per}\}$) the fields satisfy radiation conditions expressed in terms of the classical Rayleigh expansions: the scattered fields u^+ and u^- in the respective regions Ω_+ and Ω_- must be "outgoing", that is, they must admit Rayleigh expansions of the form

$$
u^+(\mathbf{x}) = \sum_{j,\ell \in \mathbb{Z}} B_{j\ell}^+ \exp[i(2\pi j \mathbf{v}_1^* + 2\pi \ell \mathbf{v}_2^* + \mathbf{k}) \cdot \tilde{\mathbf{x}}] \exp[i\gamma_{j\ell} z], \quad \mathbf{x} \in \Omega_+
\tag{49}
$$

$$
u^-(\mathbf{x}) = \sum_{j,\ell \in \mathbb{Z}} B_{j\ell}^- \exp[i(2\pi j \mathbf{v}_1^* + 2\pi \ell \mathbf{v}_2^* + \mathbf{k}) \cdot \tilde{\mathbf{x}}] \exp[-i\gamma_{j\ell} z], \quad \mathbf{x} \in \Omega_-.
\tag{50}
$$

wherein no waves in Ω_+ propagate downwards, and no waves in Ω_- propagate upwards.

Using the outgoing free-space Green function $G_k(\mathbf{z}) = \frac{e^{ik|\mathbf{z}|}}{4\pi|\mathbf{z}|}$, the scattered field u is sought in the form of a combined-field layer potential

$$
u(\mathbf{x}) = \int_{S_{per}} \frac{\partial G_k(\mathbf{x} - \mathbf{x}')}{\partial \mathbf{n}(\mathbf{x}')} \varphi_{qper}(\mathbf{x}') ds(\mathbf{x}') + i\eta \int_{S_{per}} G_k(\mathbf{x} - \mathbf{x}') \varphi_{qper}(\mathbf{x}') ds(\mathbf{x}')
\tag{51}
$$

with unknown surface density φ_{qper}. Here $\mathbf{n}$ is the outer unit normal to S_{per} and $\eta \in \mathbb{R}$ denotes a coupling constant. The unknown density φ_{qper} is the solution of the combined field integral equation

$$
\frac{1}{2}\varphi_{qper}(\mathbf{x}) + \int_{S_{per}} \frac{\partial G_k(\mathbf{x} - \mathbf{x}')}{\partial \mathbf{n}(\mathbf{x}')} \varphi_{qper}(\mathbf{x}') ds(\mathbf{x}') \quad + \quad i\eta \int_{S_{per}} G_k(\mathbf{x} - \mathbf{x}') \varphi_{qper}(\mathbf{x}') ds(\mathbf{x}')
$$
$$
= -\exp(ik\mathbf{d} \cdot \mathbf{x}), \ \mathbf{x} \in S_{per}
\tag{52}
$$

which enforces the sound-soft boundary condition under consideration. The well known term $\frac{1}{2}\varphi_{qper}$ in (52) arises as a singular contribution of the first integral in (51) in the limit as $\mathbf{x}$ approaches the boundary.

Equations (52) can be rewritten in a form that involves integration *over the reference boundary S only*. The corresponding integral equations make use of the (α, β)-quasi-periodic Green function (2), in which $\mathbf{x}$ is replaced by the difference between source and influence points,

$$
G_k^{qper}(\mathbf{x} - \mathbf{x}') = \sum_{m,n=-\infty}^{\infty} G_k((x - x, y - y') + m\mathbf{v}_1 + n\mathbf{v}_2, z - z') e^{-im\mathbf{k}\cdot\mathbf{v}_1} e^{-in\mathbf{k}\cdot\mathbf{v}_2}.
\tag{53}
$$

The integral equation (52) can equivalently be expressed in the form

$$
\frac{1}{2}\varphi_{qper}(\mathbf{x}) + \sum_{m,n \in \mathbb{Z}} \int_{S_{m,n}} \mathcal{G}(\mathbf{x} - \mathbf{x}') \varphi_{qper}(\mathbf{x}') ds(\mathbf{x}') = -\exp(ik\mathbf{d} \cdot \mathbf{x}), \ \mathbf{x} \in S_{per},
\tag{54}
$$

where

$$\mathcal{G}(\mathbf{x} - \mathbf{x}') = \frac{\partial G_k(\mathbf{x} - \mathbf{x}')}{\partial \mathbf{n}(\mathbf{x}')} + i\eta G_k(\mathbf{x} - \mathbf{x}'). \tag{55}$$

Denoting by φ the restriction of φ_{qper} to the reference boundary S and taking into account the quasi-periodicity of the density φ_{qper}, the integral equation (52) can be re-expressed in the form

$$\frac{\varphi(\mathbf{x})}{2} + \int_S \frac{\partial G_k^{per}(\mathbf{x} - \mathbf{x}')}{\partial \mathbf{n}(\mathbf{x}')} \varphi(\mathbf{x}') ds(\mathbf{x}') \quad + \quad i\eta \int_S G_k^{per}(\mathbf{x} - \mathbf{x}') \varphi(\mathbf{x}') ds(\mathbf{x}')$$
$$= -\exp(ik\mathbf{d} \cdot \mathbf{x}), \ \mathbf{x} \in S. \tag{56}$$

Thus, solution of either equation (54) or (56) produces the density $\varphi(\mathbf{x})$ which, upon insertion into (51) gives rise to the desired quasi-periodic scattered field. Note that, in view of its quasi-periodicity, the unknown φ is determined throughout S_{per} by its values on the unit cell S—and, thus, testing on S should suffice to determine φ uniquely. Indeed, the uniqueness of the problem thus posed, which is not pursued here at any length, can be established by using the periodic Green function as in equation (56) together with a proof similar to the one for the bounded obstacle case [15].

3.1 High-order evaluation of quasi-periodic layer potentials

Our Nyström approach relies on use of high-order quadratures for evaluation of the integral operators

$$(\mathcal{K}_{m,n}\varphi)(\mathbf{x}) = \int_{S_{m,n}} \mathcal{G}(\mathbf{x} - \mathbf{x}') \varphi(\mathbf{x}') ds(\mathbf{x}')$$

in equation (54) for $\mathbf{x} \in S$, where $\varphi = \varphi_{qper}$ is a quasi-periodic integral density defined on S_{per}; as noted in the previous section, testing (and thus operation evaluation) for $\mathbf{x} \in S$ suffices to determine the solution φ. Once such operators have been discretized and evaluated numerically for a given quasi-periodic function φ the solution of the problem can be obtained by means of an iterative linear algebra solver such a s GMRES [24].

We first consider a quadrature algorithm for the operator $\mathcal{K} = \mathcal{K}_{0,0}$, which is given by

$$(\mathcal{K}\varphi)(\mathbf{x}) = \int_S \mathcal{G}(\mathbf{x} - \mathbf{x}') \varphi(\mathbf{x}') ds(\mathbf{x}'), \quad \mathbf{x} \in S. \tag{57}$$

We note that this integral operator coincides with the one introduced in [8] for the problem of acoustic scattering by a *bounded obstacle* S under sound-soft boundary conditions. In fact, the algorithm we propose for evaluation of the integral operators in (56) results as an outgrowth of the fast high-order methods presented in that reference. (Extensions of these methods to sound-hard and electromagnetic problems can be found in [5] and [6].) Thus, in order to convey the main ideas underlying our periodic-structure solver, we first briefly review the algorithm [8].

The bounded-scatterer algorithm [8] evaluates the integral operator $\mathcal{K}$ in two stages, namely (a) Evaluation of the adjacent/singular interactions (i.e. integration for $\mathbf{x}'$ in areas close to $\mathbf{x}$), and (b) Accelerated evaluation of nonadjacent interactions (that is, accelerated integration for $\mathbf{x}'$ away from $\mathbf{x}$). The decomposition into adjacent and non-adjacent contributions is effected in this method by means of *floating partitions of unity*—that is, pairs of functions of the form $(\eta_{\mathbf{x}}(\mathbf{x}'), 1 - \eta_{\mathbf{x}}(\mathbf{x}'))$, where $\eta_{\mathbf{x}}$ is a windowing function with a "small" support, which equals 1 in a neighborhood of $\mathbf{x}$. Additionally, the approach [8] relies on use of smooth parametrizations of the surface S via a family of overlapping two-dimensional parameter patches $\mathcal{P}^\ell, \ell = 1, \dots P$ along with smooth mappings $\mathcal{P}^\ell$

from parameter sets $\mathcal{H}^\ell$ in two-dimensional space (where actual integrations are performed), as well as partitions of unity subordinated to the overlapping patch decomposition of the surface. i.e smooth functions w_ℓ supported on $\mathcal{P}^\ell$ such that $\sum_\ell w_\ell = 1$ throughout S. This framework allows us to reduce the integration of the density φ over the surface S to integration of smooth functions φ^ℓ compactly supported in the planar sets $\mathcal{H}^\ell$. The latter calculations require analytic resolution of weakly singular Green's functions (i.e. the order of the singularity is $\mathcal{O}(|\mathbf{x} - \mathbf{x}'|^{-1})$) which is performed via polar changes of variables (whose Jacobian cancels the Green-function singularity) together with interpolation procedures that facilitate evaluations of the surface density at radial integration points [8].

3.2 Reference acceleration cell

As indicated at the beginning of Section 3, in this paper we consider bi-periodic structures of the form (46). The present Section 3.2 constructs a certain "reference acceleration cell" (associated with the "reference domain" $\Omega = \Omega_{0,0}$) which equals a cubic domain C of side A that contains Ω. The cell C is equipped with a certain acceleration infrastructure which is based on a corresponding acceleration technique introduced in [8]. In fact, the reference acceleration cell will be utilized as an element in a method for FFT acceleration for the problem of scattering by the complete periodic structure Ω_{per}. Here and through the end of Section 3 the presentation assumes a degree of familiarity with the acceleration methodology presented in reference [8].

The acceleration infrastructure presented in that reference, which is designed to enable efficient FFT-based acceleration for the numerical evaluation of the integral operator

$$\int_S \mathcal{G}(\mathbf{x} - \mathbf{x}')\varphi(\mathbf{x}')ds(\mathbf{x}'), \quad \mathbf{x} \in S, \tag{58}$$

(the term $m = n = 0$ in (54) restricted to $\mathbf{x} \in S$) proceeds at first by partitioning the cube C into a number L^3 of identical cubic cells c_i, where L denotes an integer. The pairs (A, L) of parameters must be adjusted, if necessary, in order to ensure that the cells c_i do not admit inner acoustic resonances (eigenfunctions of the Laplace operator with homogeneous Dirichlet boundary conditions).

The acceleration algorithm [8] then constructs approximations which are obtained by substitution of the surface "true" sources within c_i (or, more precisely, of the fields that result from discrete integration of the product of the kernel $\mathcal{G}$ and the density φ for all discretization points within c_i) by "equivalent sources" on a set Π_i^ℓ ($\ell = 1, 2, 3$) which equals the union of a pair of parallel circular domains which contain the faces of c_i that are parallel to the plane $x_\ell = 0$. Clearly, there are three different such approximations. In all three cases the acoustic fields generated by the c_i-equivalent sources approximate with high order accuracy the fields produced by the true c_i sources at all cells c_j non-adjacent to c_i. The precise concept of adjacency in [8] results from a requirement that the approximation corresponding to a given cell c_i be valid, with exponentially small errors, outside a concentric cube $\mathcal{S}_i$ of side three times larger than that of c_i. For efficiency the method relies on use of equivalent sources (acoustic monopoles and dipoles) as described in what follows. For a given integral density, and for each cell c_i a set of equivalent sources (acoustic monopoles $\xi_{i,j}^{(m)\ell} G_k(\mathbf{x} - \mathbf{x}_{i,j}^\ell)$ and dipoles $\xi_{i,j}^{(d)\ell} \partial G_k(\mathbf{x} - \mathbf{x}_{i,j}^\ell)/\partial x_\ell$) placed at points $\mathbf{x}_{i,j}^\ell, j = 1, \cdots, M^{equiv}$ contained within the union of two circular domains concentric with and circumscribing the faces of c_i, whose radii are selected in accordance with the prescriptions in [8]. The fields $\psi^{c_i,true}$ radiated

by the c_i-true sources are approximated by fields $\psi^{c_i,eq}$ radiated by the c_i equivalent sources

$$\psi_{0,0}^{c_i,eq}(\mathbf{x}) = \sum_{j=1}^{\frac{1}{2}M^{equiv}} \left(\xi_{i,j}^{(m)\ell} \, G_k(\mathbf{x} - \mathbf{x}_{i,j}^\ell) + \xi_{i,j}^{(d)\ell} \frac{\partial G_k(\mathbf{x} - \mathbf{x}_{i,j}^\ell)}{\partial x_\ell} \right), \quad \mathbf{x} \notin \mathcal{S}_i. \tag{59}$$

For a given number M^{equiv} of equivalent sources (selected so as to maintain a given accuracy), the unknown monopole and dipole intensities in (59) are chosen so as to minimize in the mean-square norm the differences $(\psi^{c_i,eq}(\mathbf{x}) - \psi^{c_i,true}(\mathbf{x}))$ as $\mathbf{x}$ varies over a number n^{coll} collocation points on $\partial \mathcal{S}_i$. Hence, the intensities in (59) are obtained in practice as the least-squares solution of an overdetermined linear system $\mathbf{A}\xi = \mathbf{b}$ where $\mathbf{A}$ is an $n^{coll} \times M^{equiv}$ matrix. As discussed in Sections 3.2.2 and 3.2.3 below the method is completed via a sequence of steps which include 1) FFTs (which are used to evaluate the Cartesian convolutions that result from use of equivalent sources); 2) Correction of certain errors that arise per step 1), which are inevitable in the FFT-based operation of convolution with the Green function, and which result from "incorrect" use of equivalent sources for near interactions; and finally, 3) High-order evaluation of surface values from the values at the FFT grid. But, before such discussions we consider certain specializations of the methods above to the periodic context which, in conjunction with the windowing methodology used in this paper, have proven specially efficient.

3.2.1 Green-function contributions from periodic translates of the reference cell

It is easy to check that the set of equivalent sources for the reference scatterer Ω, as computed per the methodology described in Section 3.2, can be utilized to produce—by means of simple algegraic manipulations—the corresponding equivalent sources for any periodic translation of the unit-cell. Indeed, denoting by $(\mathcal{K}_{mn}\varphi_{qper})(\mathbf{x})$ the (m,n)-th term on the left-hand sum in equation (54) and since for $\mathbf{x} \in S$ we have $\varphi_{qper}(\mathbf{x} - m\mathbf{v}_1 - n\mathbf{v}_2) = e^{-i(m\mathbf{k}\cdot\mathbf{v}_1 + n\mathbf{k}\cdot\mathbf{v}_2)}\varphi(\mathbf{x})$, it follows that, for $\mathbf{x} \in S$,

$$\begin{aligned} (\mathcal{K}_{m,n}\varphi_{qper})(\mathbf{x}) &= e^{-i(m\mathbf{k}\cdot\mathbf{v}_1 + n\mathbf{k}\cdot\mathbf{v}_2)} \int_S \mathcal{G}(\mathbf{x} - (\mathbf{x}' - m\mathbf{v}_1 - n\mathbf{v}_2))\varphi(\mathbf{x}')ds(\mathbf{x}') \\ &= e^{-i(m\mathbf{k}\cdot\mathbf{v}_1 + n\mathbf{k}\cdot\mathbf{v}_2)} \int_S \mathcal{G}((\mathbf{x} + m\mathbf{v}_1 + n\mathbf{v}_2) - \mathbf{x}')\varphi(\mathbf{x}')ds(\mathbf{x}'). \end{aligned} \tag{60}$$

Clearly, the integral (58) evaluated at $\mathbf{x} + m\mathbf{v}_1 + n\mathbf{v}_2$ coincides with the last integral in equation (60), and, therefore, this last integral is approximated closely by the equivalent-source expression $\psi_{0,0}^{c_i,eq}(\mathbf{x} + m\mathbf{v}_1 + n\mathbf{v}_2)$ where $\psi_{0,0}^{c_i,eq}$ is defined in equation (59). It follows that the quantity $(\mathcal{K}_{mn}\varphi_{qper})(\mathbf{x})$ can in turn be approximated closely by

$$\begin{aligned} \psi_{m,n}^{c_i,eq}(\mathbf{x}) \quad &:= \quad e^{-i(m\mathbf{k}\cdot\mathbf{v}_1 + n\mathbf{k}\cdot\mathbf{v}_2)}\psi_{0,0}^{c_i,eq}(\mathbf{x} + m\mathbf{v}_1 + n\mathbf{v}_2) = \sum_{j=1}^{\frac{1}{2}M^{equiv}} e^{-i(m\mathbf{k}\cdot\mathbf{v}_1 + n\mathbf{k}\cdot\mathbf{v}_2)} \\ &\times \quad \left(\xi_{i,j}^{(m)\ell} \, G_k(\mathbf{x} - \mathbf{x}_{i,j}^\ell + m\mathbf{v}_1 + n\mathbf{v}_2) + \xi_{i,j}^{(d)\ell} \frac{\partial G_k(\mathbf{x} - \mathbf{x}_{i,j}^\ell + m\mathbf{v}_1 + n\mathbf{v}_2)}{\partial x_\ell} \right). \end{aligned} \tag{61}$$

Calling $\psi^{c_i,eq}(\mathbf{x})$ the sum of the quantities $\psi_{m,n}^{c_i,eq}(\mathbf{x})$ over all integers m and n, in view of equation (61) we have

$$\psi^{c_i,eq}(\mathbf{x}) := \sum_{m,n=-\infty}^{\infty} \psi_{m,n}^{c_i,eq}(\mathbf{x}) = \sum_{j=1}^{\frac{1}{2}M^{equiv}} \left(\xi_{i,j}^{(m)\ell} \, G_k^{qper}(\mathbf{x} - \mathbf{x}_{i,j}^\ell) + \xi_{i,j}^{(d)\ell} \frac{\partial G_k^{qper}(\mathbf{x} - \mathbf{x}_{i,j}^\ell)}{\partial x_\ell} \right)$$

15

provides a close approximation of the quantity

$$\sum_{m,n\in\mathbb{Z}}\int_{S_{m,n}}\mathcal{G}(\mathbf{x}-\mathbf{x}')\varphi_{qper}(\mathbf{x}')ds(\mathbf{x}'),\quad \mathbf{x}\notin\mathcal{S}_i. \tag{62}$$

The approximating expression (62) contains the quasi-periodic Green's function G_k^{qper}, and it at this point that the proposed accelerated algorithm utilizes the windowed periodic Green function: replacing G_k^{qper} in this expression by its windowed approximation

$$\begin{aligned}
G^a(\mathbf{x}-\mathbf{x}') &= \frac{1}{4\pi}\sum_{m,n\in\mathbb{Z}}\frac{e^{ik\left(\|(x_1-x_1',x_2-x_2')+m\mathbf{v}_1+n\mathbf{v}_2\|^2+(x_3-x_3')^2\right)^{1/2}}}{\left(\|(x_1-x_1',x_2-x_2')+m\mathbf{v}_1+n\mathbf{v}_2\|^2+(x_3-x_3')^2\right)^{1/2}} \\
&\times\ e^{-i(m\mathbf{k}\cdot\mathbf{v}_1+n\mathbf{k}\cdot\mathbf{v}_2)}\chi\left(\tfrac{\|(x_1-x_1',x_2-x_2')+m\mathbf{v}_1+n\mathbf{v}_2\|}{a}\right),
\end{aligned} \tag{63}$$

which, as established in Theorem 2.1, gives rise to super-algebraic convergence as $a\to+\infty$, we obtain the corresponding super-algebraically close approximation

$$\psi^{c_i,eq}(\mathbf{x}):=\sum_{j=1}^{\frac{1}{2}M^{equiv}}\left(\xi_{i,j}^{(m)\ell}\,G^a(\mathbf{x}-\mathbf{x}_{i,j}^\ell)+\xi_{i,j}^{(d)\ell}\frac{\partial G^a(\mathbf{x}-\mathbf{x}_{i,j}^\ell)}{\partial x_\ell}\right)\ \text{for }(i,x)\text{ such that }\mathbf{x}\notin\mathcal{S}_i. \tag{64}$$

(Note that the k dependence is explicitly displayed in the notation G_k for the free-space Green function, but, for notational simplicity, it is suppressed in the notation G^a for the windowed periodic Green function used in, e.g., equation (64).) Since for a given ℓ the circular regions Π_i^ℓ are not pairwise disjoint, it is necessary, as indicated in [8], to combine equivalent source intensities for sources supported at a given point $\mathbf{x}'$ that corresponds to two different cells, say, c_r and c_s for which $\mathbf{x}'=\mathbf{x}_{r,p}^\ell=\mathbf{x}_{s,q}^\ell$ for some integers p and q. We thus define the quantities

$$\psi^{(*)\ell}(\mathbf{x})=\sum_{\mathbf{x}'\in\Pi^\ell}\left(\xi_{\mathbf{x}'}^{(m)\ell}G^a(\mathbf{x}-\mathbf{x}')+\xi_{\mathbf{x}'}^{(d)\ell}\frac{\partial G^a(\mathbf{x}-\mathbf{x}')}{\partial x_\ell'}\right) \tag{65}$$

where $\xi_{\mathbf{x}'}^{(m)\ell}$ and $\xi_{\mathbf{x}'}^{(d)\ell}$ denote the sum of all intensities of equivalent sources located at a point $\mathbf{x}'\in\Pi^\ell$:

$$\xi_{\mathbf{x}'}^{(m)\ell}=\sum_{\mathbf{x}_{i,j}^\ell=\mathbf{x}'}\xi_{i,j}^{(m)\ell}\quad\xi_{\mathbf{x}'}^{(d)\ell}=\sum_{\mathbf{x}_{i,j}^\ell=\mathbf{x}'}\xi_{i,j}^{(d)\ell}.$$

Note that, while the quantity $\psi^{(*)\ell}$ contains contributions from cells c_i for which the far-field restriction $\mathbf{x}\notin\mathcal{S}_i$ is not satisfied, the algorithmic evaluation of the quantity (64) does proceed by evaluating $\psi^{(*)\ell}$ (by means of an FFT) and then correcting for nearby contributions $\mathbf{x}\in\mathcal{S}_i$. These two steps in the algorithm are considered in the following subsections.

3.2.2 FFT evaluation of the convolutions and Correction step

As indicated above, the inaccurate quantity $\psi^{(*)\ell}(\mathbf{x})$ (equation (65)) plays an important role in the proposed accelerated quasi-periodic solver. For each $\ell=1,2,3$ the proposed algorithm first evaluates the Cartesian convolutions $\psi^{(*)\ell}(\mathbf{x})$ ($\mathbf{x}\in\Pi^\ell$) by means of the three-dimensional FFT algorithm. The proposed use of the quasi-periodic Green function, which only occurs in the algorithm as part of the acceleration step, provides the additional advantage that, under the strategies

16

mentioned in Section 3.3, the Green function needs to be evaluated at a number of the order of $\mathcal{O}(N^{4/3})$ points only—and not for the $\mathcal{O}(N^2)$ pairs of discretization points, where $\mathcal{O}(N)$ is the number of grid points that are used to discretize the scatterers in the reference cell. As demonstrated in Section 4, the combined windowed-Green-function FFT-based algorithm provides a very efficient quasi-periodic solver—at least away from Wood anomalies.

But, as indicated above, corrections are necessary to the pure FFT-based quantity $\psi^{(*)\ell}(\mathbf{x})$: the incorrect contributions $\mathbf{x} \in \mathcal{S}_i$ must be subtracted, and corresponding accurate replacements need to be added. In some detail, the quantity $\psi^{(na,eq)\ell}(\mathbf{x})$, which equals the sum of the values at the point $\mathbf{x} \in S$ of all fields arising from equivalent sources nonadjacent to c_i can be obtained by subtracting from $\psi^{(*)\ell}(\mathbf{x})$ the field arising at $\mathbf{x}$ from equivalent sources located within $\mathcal{S}_i$, where i is the index for which $\mathbf{x} \in c_i$. The "corrections" necessary to produce $\psi^{(na,eq)\ell}(\mathbf{x})$ from $\psi^{(*)\ell}(\mathbf{x})$ can also be evaluated efficiently, by means of a sequence of (small) three-dimensional FFTs, since they only involve (small) three-dimensional convolutions and *free-space Green's functions*. Once completed for $\ell = 1$, 2, 3, this overall procedure results in accurate values, on a mesh that samples the boundaries of all cells c_i, of the fields arising from all true sources contained in all cells c_j not adjacent to c_i.

In order to obtain approximations of the nonadjacent interactions $\psi^{(na,true)}(\mathbf{x})$ (that is, the fields generated at $\mathbf{x}$ by the true discrete surface sources contained outside $\mathcal{S}_i$) at surface points $\mathbf{x} \in S \cap c_i$, the algorithm employs solutions to the Helmholtz equation within c_i, with Dirichlet boundary conditions given by $\psi^{(na,eq)\ell}$, $\ell = 1$, 2, 3. These Dirichlet problems can be solved uniquely (in view of our assumption that the wavenumber k is not a resonant frequency), and thus the good approximation properties of the nonadjacent interactions on the boundary of each cell c_i translate into good approximations for the nonadjacent interactions on the surface S. Following [8], our algorithm produces the needed solutions of Dirichlet problems by means of approximations of the form

$$P(\mathbf{x}) = \sum_{j=1}^{n^w} \gamma^j \exp(ik\mathbf{u}_j \cdot \mathbf{x}), \tag{66}$$

valid within c_i (in terms of plane wave solutions of the Helmholtz equation), for the field $\psi^{(na,true)}$. Here $\mathbf{u}_j$ are unit vectors that adequately sample the surface of the unit sphere, and the coefficients γ^j are obtained in such a way that the relation $P(\mathbf{x}) = \psi^{(na,true)}(\mathbf{x})$ is satisfied, in the least-squares sense, for all $\mathbf{x}$ in an adequately chosen collocation mesh on the cubic surface $\mathcal{S}_i$.

3.2.3 Adjacent interactions

Having evaluated, by means of FFTs and plane wave expansions, accurate approximations of the surface values of the field $\psi^{(na,true)}(\mathbf{x})$ produced by the non-adjacent surface sources (for all discretization points $\mathbf{x} \in S$), surface values of the *total field* are then obtained by direct addition of necessary singular and non-singular adjacent surface sources. Briefly, the fields that need to be added to (the approximations just obtained for) the field $\psi^{(na,true)}(\mathbf{x})$ (for a point $\mathbf{x} \in S$) include (i) Adjacent regular sources, that is, trapezoidal-rule contributions to the integral operator from sources lying outside the support of the floating POU $\eta_{\mathbf{x}}$ but inside $\mathcal{S}_i$ (none of which are included in $\psi^{(na,true)}(\mathbf{x})$), and (ii) Adjacent singular sources, that is, the local contributions to the integral operator considered in stage (a) of Section 3.1.

3.3 Computational cost

It is easy to estimate the computational cost of the proposed windowed-Green-function/accelerated algorithm for quasi-periodic scattering problems. Indeed, the cost of the algorithm is the same as that of its non-periodic counterpart [8] except for the fact that, in the present case, the use of the equivalent-source intensities requires values of the *quasi-periodic Green function G^a*, as shown in equation (65), instead of the use of the free-space Green function G_k in the former algorithm. (Note that the equivalent sources themselves are obtained, even in the present periodic context, by means of the *free-space Green function G_k*, as shown in equation (59).) The operation count now proceeds simply. The algorithm [8] is reported to require a cost of $\mathcal{O}(N^{4/3} \log N)$ operations. In addition, the windowed-Green function accelerated algorithm requires a precomputation of the Green function $G^a(\mathbf{x})$ and its derivatives along each coordinate direction, and at all points $\mathbf{x}$ in the accelerator meshes $\Pi^\ell, \ell = 1, 2, 3$. These precomputations are performed by direct summation at a cost of $\mathcal{O}(a^2 N^{4/3})$ operations. The overall cost of the algorithm, including all necessary Green function evaluations, thus amounts to the $\mathcal{O}(a^2 N^{4/3})$ precomputation cost plus the necessary number of GMRES iterations at a cost of $\mathcal{O}(N^{4/3})$ each.

4 Numerical results

To demonstrate the speed and accuracy of the proposed accelerated Nÿstrom algorithm we present results of applications of this method to problems of scattering by doubly periodic arrays of perfectly-conducting obstacles at non-Wood configurations. For simplicity we consider two dimensional rectangular lattices of scatterers, that is $\mathbf{v}_1 = d_1(1, 0, 0)$ and $\mathbf{v}_2 = d_2(0, 1, 0)$; results of similar quality have been produced for general lattices. We present two main accuracy indicators, namely certain convergence studies on one hand, and departure from energy conservation in the numerical solution, on the other. The latter test, which derives from the energy conservation result satisfied by the exact PDE solution for the perfectly conducting scatterers under consideration—namely, that the energy flux of the incident field must equal the sum of the energy fluxes of the reflected field and the transmitted field—can be expressed in terms of the Rayleigh coefficients $B_{j,\ell}^+$ of the scattering problem:

$$\sum_{(j,\ell)\in P} \gamma_{j\ell} |B_{j,\ell}^+|^2 + \sum_{(j,\ell)\in P} \gamma_{j\ell} |B_{j,\ell}^- + \delta_{j,\ell}^{0,0}|^2 = \gamma_{00}, \tag{67}$$

where P is the set of propagating harmonics $P = \{(j, \ell) : \|\mathbf{v}_{j\ell}^*\| < k^2\}$, where $\gamma_{j\ell}$ are defined in equation (7). The energy defect for numerically computed Rayleigh coefficients $\widetilde{B}_{r,s}^{\pm}$ is then defined as

$$\varepsilon = \frac{\left| \sum_{(j,\ell)\in P} \gamma_{j\ell} \left(|\widetilde{B}_{j,\ell}^+|^2 + |\widetilde{B}_{j,\ell}^- + \delta_{j,\ell}^{0,0}|^2 \right) - \gamma_{0,0} \right|}{\gamma_{0,0}} \tag{68}$$

(where $\delta_{j,\ell}^{0,0}$ equals 1 for $(j, \ell) = (0, 0)$ and zero otherwise). Experiments based on fully converged solutions (as verified by means of convergence studies), suggest that the energy defect is an excellent indicator of solution accuracy for the integral solvers under consideration.

All of the numerical examples presented in this section concern problems of scattering by periodic arrangements of either spherical or bean-shaped scatterers [8], both of which have diameter equal to 2. In all cases the periods are given by $d_1 = d_2 = 4$, and plane-wave incident fields with incidence angles $\psi = \phi = 0$ (that is, normal incidence) and $\psi = \phi = \pi/3$ (oblique incidence) are

Scatterer	k	Unknowns	a	ε	ε_1	Iter
Sphere	1	$6 \times 64 \times 64$	25	1.1×10^{-3}	1.9×10^{-3}	11
Sphere	1	$6 \times 64 \times 64$	50	1.2×10^{-4}	6.1×10^{-5}	11
Sphere	1	$6 \times 64 \times 64$	75	5.0×10^{-6}	2.1×10^{-6}	11
Sphere	1	$6 \times 64 \times 64$	150	3.8×10^{-7}	3.5×10^{-8}	11

Table 1: Convergence of the periodic solvers using G^a for increasing values of the truncation radius a for doubly periodic arrays of spheres under normal incidence. The reference solution corresponds to $a = 400$, in which case the conservation of energy error was $\varepsilon = 1.2 \times 10^{-7}$.

considered. For these experiments we have used the accelerator parameters $L = 3$, $M^{equiv} = 4$, $n^{coll} = 8$, and $n^w = 4$. In all cases the linear systems resulting from our discretization was solved by means of the GMRES iterative solver with a relative residual tolerance Tol. The tolerance value $Tol = 10^{-8}$ was used to produce Table 1 while the less restrictive "adequate-accuracy" tolerance 10^{-4} was used for Tables 2 and 3. Table 1 showcases the high-order accuracy achieved by our periodic solvers in the case of bi-periodic arrays of spheres under normal incidence. Tables 2 and 3 present results for periodic arrays of spheres and bean-shaped obstacles for various wavenumbers k and various values of the window-radius a.

The errors ε presented in these tables was evaluated in accordance with equation (68). The error ε_1, on the other hand, was calculated as the absolute error in the Rayleigh coefficient $B_{0,0}^+$ (as estimated by comparison with a reference solution obtained by means of a highly-refined discretization, a large value a and a sufficiently small tolerance Tol). We also report numbers of iterations and computational times required by the GMRES solvers to reach the tolerance Tol in each case. The results were obtained by means of a C++ implementation of our solvers on a single core of a 2.67 GHz Intel Xeon CPU with 24Gb of RAM.

5 Conclusions

This paper demonstrates that the previous two-dimensional windowed Green-function methodology [4] for quasi-periodic scattering problems can successfully be extended to the three-dimensional context. In particular, this paper presents the first rigorous proof of super-algebraic convergence of the windowed Green-function method in three-dimensional space. An accelerated windowed Green-function algorithm is presented, which possesses excellent properties. Comparisons, in simple examples, with one of the most advanced techniques for evaluation of periodic Green functions [17] (which is based on a combination of resummation and partitioning techniques) suggests that the proposed methodology can be orders of magnitude less expensive than former approaches.

References

[1] Barnett, Alex and Greengard, Leslie, *A new integral representation for quasi-periodic scattering problems in two dimensions*, J. Comp. Phys., 229, 6898–6914 (2010).

Scatterer	k	N	a	ε	ε_1	Iter	Computational Times		
							Set-up	Time/It	Total
Sphere	0.75	1350	20	5.0×10^{-3}	6.4×10^{-3}	5	14sec	0.4sec	16sec
Sphere	0.75	1350	30	4.7×10^{-4}	1.6×10^{-3}	5	29sec	0.4sec	31sec
Sphere	0.75	1350	40	2.4×10^{-5}	2.2×10^{-4}	5	51sec	0.4sec	53sec
Sphere	9	5766	20	5.0×10^{-3}	3.6×10^{-3}	13	14sec	3.4sec	57sec
Sphere	9	5766	30	1.1×10^{-3}	1.3×10^{-3}	13	29sec	3.4sec	1m14sec
Sphere	9	5766	40	7.0×10^{-5}	2.1×10^{-4}	13	51sec	3.4sec	1m35sec
Bean	0.75	1350	20	3.3×10^{-3}	5.5×10^{-3}	10	14sec	1.2sec	26sec
Bean	0.75	1350	30	1.9×10^{-3}	1.4×10^{-3}	10	29sec	1.2sec	42sec
Bean	0.75	1350	40	3.2×10^{-4}	3.4×10^{-4}	10	51sec	1.2sec	1m5sec
Bean	9	5766	20	6.1×10^{-3}	4.0×10^{-3}	17	14sec	5.35sec	1m45sec
Bean	9	5766	30	1.1×10^{-3}	9.9×10^{-4}	17	29sec	5.35sec	2m0sec
Bean	9	5766	40	3.2×10^{-5}	1.7×10^{-4}	17	51sec	5.35sec	2m30sec

Table 2: Convergence of the periodic solvers using G^a for increasing values of the truncation radius a for doubly periodic arrays of spherical and bean-shaped scatterers under normal incidence.

Scatterer	k	N	a	ε	ε_1	Iter	Computational Times		
							Set-up	Time/It	Total
Sphere	9	5766	20	8.0×10^{-3}	5.2×10^{-3}	23	14sec	3.4sec	1m31sec
Sphere	9	5766	30	3.7×10^{-3}	8.0×10^{-4}	22	29sec	3.4sec	1m44sec
Sphere	9	5766	50	4.5×10^{-5}	1.7×10^{-4}	22	1m25sec	3.4sec	2m40sec
Bean	9	5766	20	4.4×10^{-3}	7.8×10^{-3}	21	14sec	5.35sec	2m6sec
Bean	9	5766	30	1.2×10^{-3}	3.1×10^{-3}	21	29sec	5.35sec	2m23sec
Bean	9	5766	50	3.0×10^{-5}	2.1×10^{-4}	21	1m25sec	5.35sec	3m17sec

Table 3: Convergence of the periodic solvers using G^a for increasing values of the truncation radius a for doubly periodic arrays of spherical and bean-shaped scatterers under oblique incidence $\phi = \psi = \pi/3$.

[2] Bleszynski, E. H., Bleszynski, M. K., and Jaroszewicz, T., *Rigorous modeling of electromagnetic wave interactions with large dense discrete scatterers*, in Ultra-Wideband, Short Pulse Electromagnetics 9, Part 1, 65–77, DOI: 10.1007/978-0-387-77845-7_8 (2010).

[3] J. M. Borwein, M. L. Glasser, R. C. McPhedran, J. G. Wan, and I. J. Zucker, *Lattice Sums Then and Now* in *Encyclopedia of Mathematics and its Applications*, Vol. 150 (2013)

[4] O. P. Bruno and B. Delourme, *Rapidly convergent two-dimensional quasi-periodic Green function throughout the spectrum—including Wood anomalies* J. Comp. Phys., 262, 262–290 (2014).

[5] Bruno, O., Elling, T., Paffenroth, R., Turc, C., *Electromagnetic integral equations requiring small numbers of Krylov-subspace iterations*, J. Comput. Phys, 228 (17), 2009, 6169-6183.

[6] Bruno, O., Elling, T., Turc, C., *Regularized integral equations and fast highorder solvers for soundhard acoustic scattering problems*, International Journal for Numerical Methods in Engineering, 91 (10), 2012, 1045-1072.

[7] O. P. Bruno and B. Delourme, 2D-Rapidly convergent quasi-periodic Green function for the scattering of acoustic waves from rough surfaces throughout the spectrum including Wood Anomalies. Waves Conference Proceedings, Tunis, Tunisia, June 3-7 2013.

[8] Bruno, O. P. and Kunyansky, L., "A fast, high-order algorithm for the solution of surface scattering problems: basic implementation, tests and applications", *J. Computat. Phys. 169*, (2001) pp. 80–110.

[9] Bruno, O., and L. Kunyansky, *Surface scattering in three dimensions: an accelerated high-order solver*, R. Soc. Lon. Proc. Ser. A Math. Phys. Eng. Sci., 2016, 2921–2934 (2001).

[10] Bruno, Oscar P. and Reitich, Fernando, *Solution of a boundary-value problem for the Helmholtz equation via variation of the boundary into the complex domain*, Proc. R. Soc. Edinburgh, 122A, 317–340 (1992).

[11] O. P. Bruno, S. Shipman, C. Turc, and S. Venakides, Efficient Evaluation of Doubly Periodic Green Functions in 3D Scattering, Part II: Wood Anomaly Frequencies

[12] O. P. Bruno, S. Shipman, C. Turc, and S. Venakides, *Efficient Solution of Acoustic and Electromagnetic Scattering Problems in Three-Dimensional Periodic Media.* Waves Conference Proceedings, Vancouver, Canada, July 25-29 2011.

[13] Capolino, F., Wilton, D. R., and Johnson, W. A., *Efficient computation of the 3D Greens function for the Helmholtz operator for a linear array of point sources using the Ewald method*, J. Comp. Phys., 223, 250–261 (2007).

[14] Chen, Xinfu and Friedman, Avner, *Maxwell's Equations in a Periodic Structure*, Trans. Am. Math. Soc., 323(2) 465–507 (1991).

[15] D. Colton and R. Kress. *Integral Equation Methods in Scattering Theory.* John Wiley & Sons, 1983.

[16] Ewald, P. P., *Die Berechnung optischer und elektrostatischer Gitterpotentiale* Annalen der Physik, 369(3), 253–287 (1921).

[17] Guerin, S., Enoch, S., and G. Tayeb, *Combined method for the computation of the doubly periodic Green functions*, Journal of Electromagnetic Waves and Applications, Vol. 15, 205–221 (2001).

[18] Linton, C. M., *Lattice Sums for the Helmholtz Equation*, SIAM Rev., 52(4), 630–674 (2010).

[19] Monro, John A., *A Super-Algebraically Convergent, Windowing-Based Approach to the Evaluation of Scattering from Periodic Rough Surfaces*, Ph.D. dissertation, Cal. Tech., 2007.

[20] Maystre, D., *Integral methods* in *Electromagnetic Theory of Gratings*, Ch. 3. R. Petit, ed., 63–100 (1980).

[21] Nevière, M., *The homogeneous problem* in *Electromagnetic Theory of Gratings*, Ch. 5. R. Petit, ed., 123–157 (1980).

[22] Papanicolaou, V. G., *Ewald's method revisited: rapidly convergent series representations of certain Green's functions*, J. Comp. Anal. Appl. 1 (1) 105-114 (1999).

[23] Lord Rayleigh, *Note on the remarkable case of diffraction spectra described by Prof. Wood*, Philos. Mag., Vol. 14, 60–65 (1907).

[24] Saad, Y., and M. H. Schultz, "GMRES: A generalized minimal residual algorithm for solving non-symmetric linear systems", *SIAM J. Sci. Stat. Comput., 3*, vol. 7, 1986, 856–869.

[25] Veysoglu, M. E., Yueh, H. A., Shin, R. T., and Kong, J. A., *Polarimetric passive remote sensing of periodic surfaces*, J. Electromagn. Waves Appl., Vol. 5, 267–280 (1991).

[26] Wood, R. W., *On a remarkable case of uneven distribution of light in a diffraction grating spectrum*, Philos. Mag., Vol. 4, 396–402 (1902).